We are IntechOpen, the world's leading publisher of Open Access books Built by scientists, for scientists

6,900
Open access books available

185,000
International authors and editors

200M
Downloads

Our authors are among the

154
Countries delivered to

TOP 1%
most cited scientists

12.2%
Contributors from top 500 universities



WEB OF SCIENCE™

Selection of our books indexed in the Book Citation Index in Web of Science™ Core Collection (BKCI)

Interested in publishing with us?
Contact book.department@intechopen.com

Numbers displayed above are based on latest data collected.
For more information visit www.intechopen.com



Chapter 23

Ionic Liquids Facilitate the Development of Absorption Refrigeration

Shiqiang Liang, Wei Chen, Yongxian Guo and Dawei Tang

Additional information is available at the end of the chapter

http://dx.doi.org/10.5772/58982

1. Introduction

The rapid progress in the development of ionic liquids has generated enthusiasm for their application in many traditional fields and renewed interest in absorption refrigeration. New absorption refrigeration working pairs containing ionic liquids have gained widespread attention in the past decade. In a chapter entitled "The Latent Application of Ionic Liquids in Absorption Refrigeration" [1] that we have published 3 years ago with InTech in the book entitled "Applications of Ionic Liquids in Science and Technology" achieved impressive readership results and has so far been accessed more than 4000 times. Over the past 3 years, progress in this field has been outstanding, and a few commercially competitive new working pairs were discovered. In this chapter, we describe the latest progress in the development of a few mentionable new working pairs containing ionic liquids for absorption refrigeration and a type of completely new conceptual absorption refrigeration working pair that was proposed by us and is expected to lead to a major breakthrough in the development of absorption refrigeration.

2. Recent progress in absorption refrigeration working pairs containing ionic liquids

In the past 3 years, enthusiasm for studies on absorption refrigeration working pairs containing ionic liquids seems to have waned. The once preferred ionic liquid working pairs, such as Freon-IL, CO_2-IL, and NH_3-IL, do not receive attention from researchers any longer. However, some impressive progress is still being made for working pairs composed of a refrigerant and [RR'Im]DMP (1-R,3-R'-imidazolium dimethylphosphate).

INTECH
open science | open minds

© 2015 The Author(s). Licensee InTech. This chapter is distributed under the terms of the Creative Commons Attribution License (http://creativecommons.org/licenses/by/3.0), which permits unrestricted use, distribution, and eproduction in any medium, provided the original work is properly cited.

2.1. [mmIm]DMP-CH_3OH

Zhao Jie et al. [2] measured the saturation vapor pressure of [mmIm]DMP-CH_3OH at T = 303.15–363.15 K and over a low methanol mole fraction range for x including 0.529, 0.558, 0.582 and 0.605. Zhao Jin et al. [3] measured the saturation vapor pressure of [mmIm]DMP-CH_3OH at T = 280–370 K and over the high methanol mole fraction range for x including 0.8222, 0.9123, 0.9418 and 0.9652. These experimental results were confirmed by Chen et al. [4] using the UNIFAC model and the Wilson model to predict the vapor pressure and the excess enthalpy, respectively. Figs. 1 and 2 show the predicted vapor pressure and excess enthalpy, respectively, at T = 280–380 K and x = 0–1.

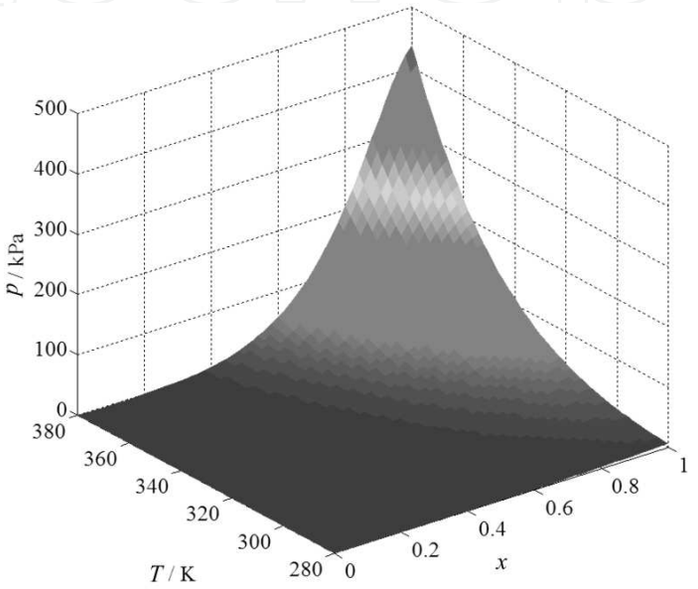


Figure 1. The predicted vapor pressure of [mmIm]DMP-CH_3OH.

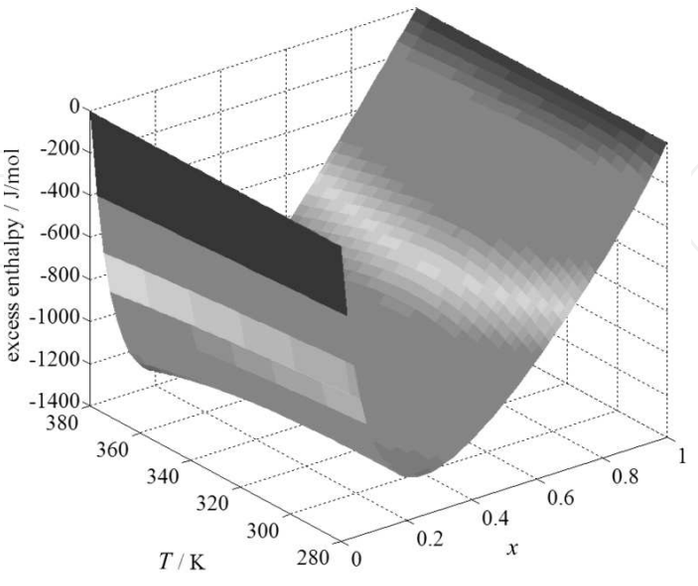


Figure 2. The predicted excess enthalpy of [mmIm]DMP-CH_3OH.

http://dx.doi.org/10.5772/58982

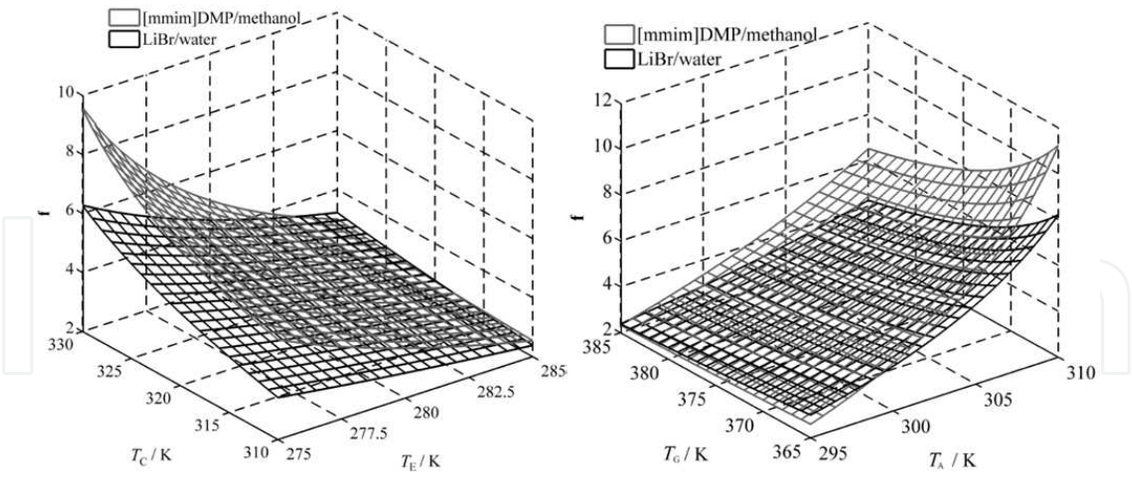


Figure 3. Effects of operating temperatures on the *f* of the [mmIm]DMP-CH_3OH system.

The thermodynamic performances of single effect [mmIm]DMP-CH_3OH absorption refrigeration have been simulated and analyzed. Fig. 3 shows the effects of the operating temperatures [condensing temperature (T_C), evaporating temperature (T_E), generating temperature (T_G), and absorption temperature (T_A)] on the circulation ratio, *f*, of the single system. From Fig. 3, the *f* of [mmIm]DMP-CH_3OH is higher than that of LiBr/H_2O but still acceptable for operation, and the coefficient of performance (COP) of the [mmIm]DMP-CH_3OH absorption refrigeration will remain good, if the heat transfer areas of the regenerator are designed appropriately.

Fig. 4 shows the effects of the operating temperatures on the COP of the single system. From Fig. 4, the COP of the [mmIm]DMP-CH_3OH absorption refrigeration is lower than that of LiBr/H_2O absorption refrigeration under the same temperature conditions, but higher than that of H_2O/NH_3 absorption refrigeration under most temperature conditions. When the heat source temperature is greater than 400 K, [mmIm]DMP-CH_3OH absorption is still possible with a high COP close to that of LiBr/H_2O absorption refrigeration. In general, [mmim]DMP/methanol has excellent potential for application as the working pair in absorption refrigeration.

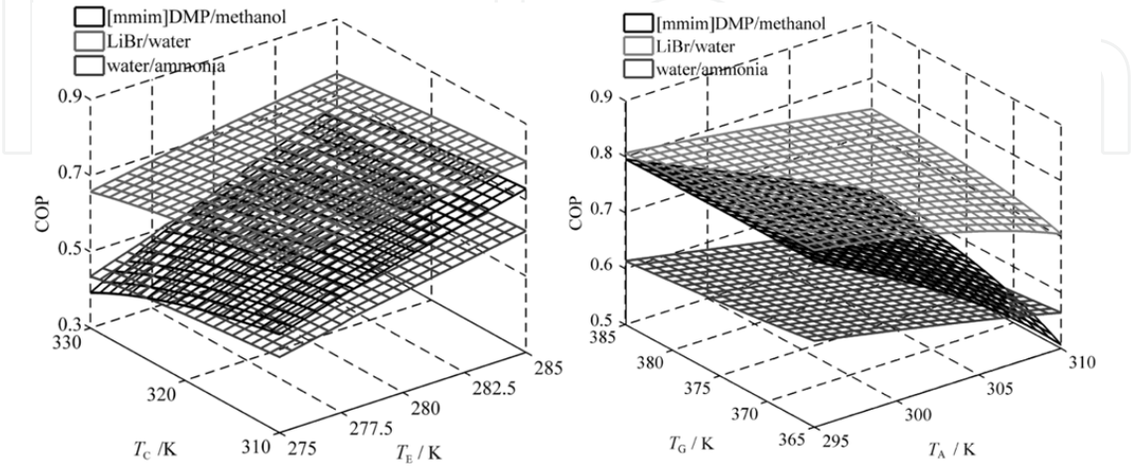


Figure 4. Effects of operating temperatures on the COP of the [mmIm]DMP-CH_3OH system.

2.2. [dmIm]DMP-H_2O

Dong et al. [5] studied the thermophysical properties of the [dmIm]DMP-H_2O system. The vapor pressures of the [dmIm]DMP-H_2O system at mass fractions of ionic liquids, ω, in the range of 0.10 to 0.90 were measured and correlated using a non-random two-liquid (NRTL) model. The experimental data and the model predictions are presented in Fig. 5.

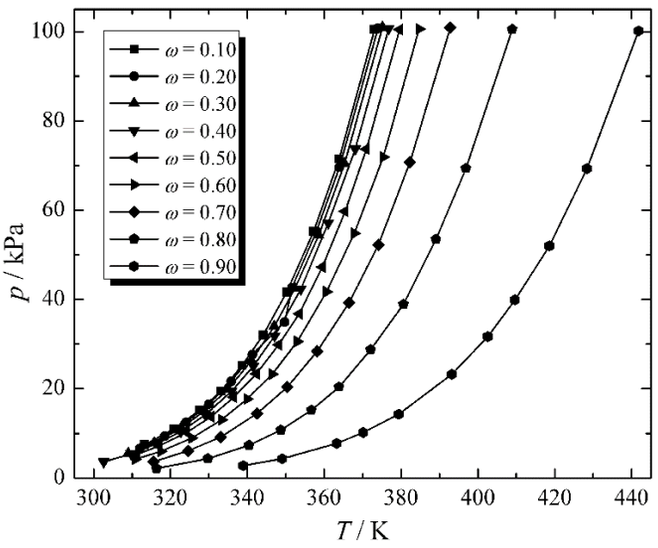


Figure 5. Vapor pressures of [dmIm]DMP-H_2O.

The heat capacities of [dmIm]DMP-H_2O at a ω in the range of 0.10 to 0.90 and a temperature range of 303.15–353.15 K were determined by a BT2.15 Calvet microcalorimeter. Fig. 6 presents the experimental data and the corresponding correlation results.

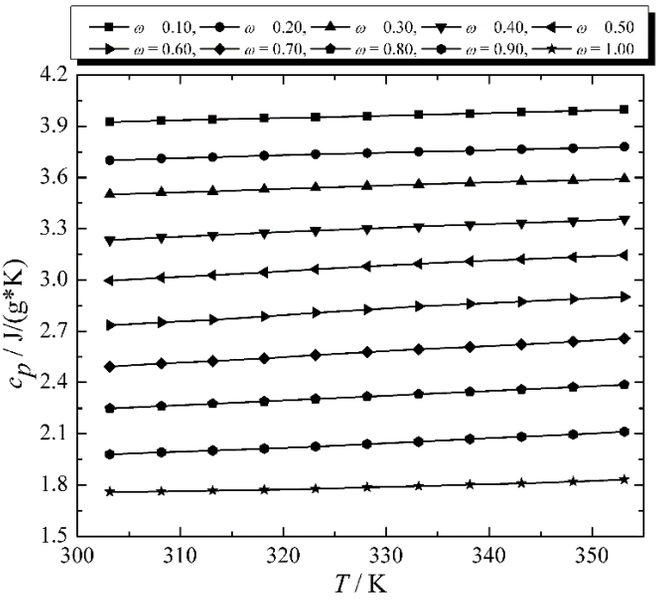


Figure 6. Heat capacities of [dmIm]DMP-H_2O.

http://dx.doi.org/10.5772/58982

The performance characteristics of [dmIm]DMP-H_2O and LiBr-H_2O single effect absorption refrigeration at t_E = 10 °C, t_C = 40 °C, t_A = 30 °C, and t_G = 80 °C were calculated and are listed in Table 1. It can be seen that the COP of the [dmIm]DMP-H_2O system is slightly lower than but close to that of the traditional working pair LiBr-H_2O.

Working pair	ω_2	ω_1	f	COP
[dmIm]DMP-H_2O	0.867	0.768	8.77	0.829
LiBr-H_2O	0.537	0.486	6.59	0.835

Table 1. Comparison of performance characteristics between the [dmIm]DMP-H_2O and LiBr-H_2O systems

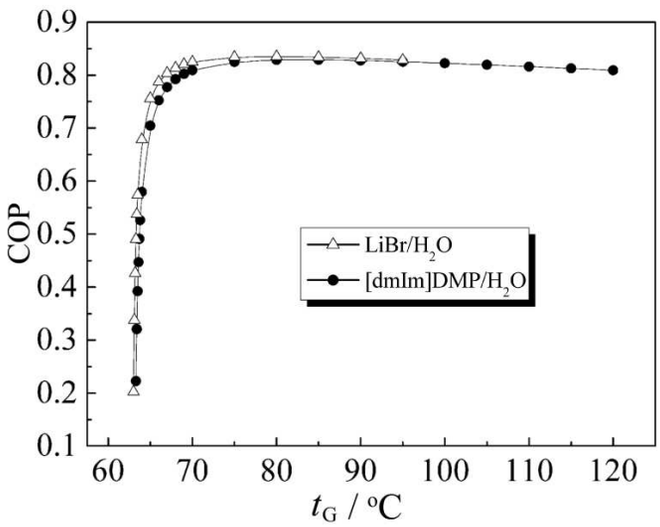


Figure 7. Effects of t_G on the COPs of the [dmIm]DMP-H_2O and LiBr-H_2O systems.

Fig. 7 shows the effects of changes in the t_G on the COP for the [dmIm]DMP-H_2O and LiBr-H_2O systems with t_E = 10 °C, t_C = 40 °C, and t_A = 30 °C. It can be seen that as the t_G is increased, the COPs of the [dmIm]DMP-H_2O and LiBr-H_2O systems stabilize after a sharp rise, and there is an optimum t_G, at which the COP reaches the highest value. When reaching the stable stage, the COP of the [dmIm]DMP-H_2O system is very close to that of the LiBr-H_2O system. Moreover, the operating temperature range has been extended and operational safety has been achieved for the [dmIm]DMP-H_2O working pair, because it has no limitation of crystallization. These findings indicate that [dmIm]DMP-H_2O has the potential to be novel working pair for absorption refrigeration.

2.3. [emIm]DMP-H_2O

Ren et al. [6] measured the vapor pressure of the [emIm]DMP-H_2O binary system at different IL mole fractions, x, ranging from 0.1 to 0.5, and the experimental data were fitted using the NRTL model (Fig. 8).

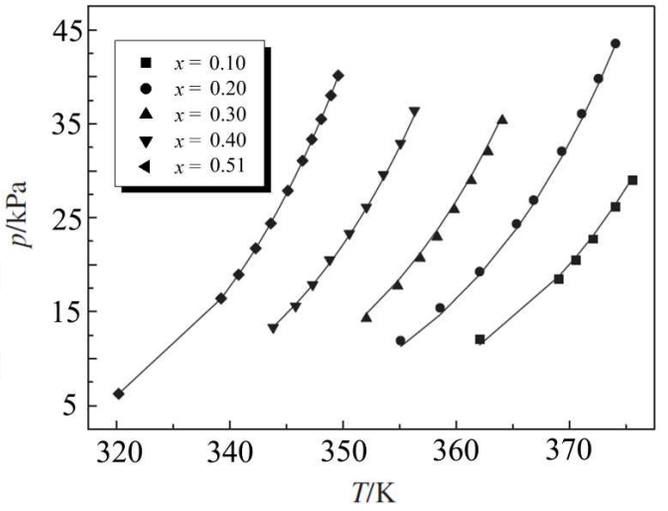


Figure 8. Vapor pressure of [emIm]DMP-H_2O with different mole fractions of IL and at different temperatures.

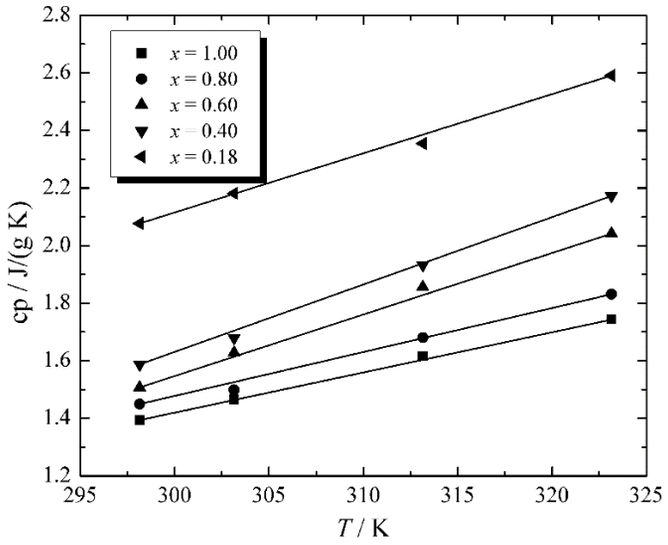


Figure 9. Specific heat capacities of [emIm]DMP-H_2O with different mole fractions of IL and at different temperatures.

The specific heat capacities of the [emIm]DMP-H_2O binary system were also measured at T = 298.15–323.15 K and with different IL mole fractions, x, ranging from 0.18 to 1. Fig. 9 presents the experimental data and the model predictions.

Based on the above thermophysical properties, Zhang et al. [7] investigated the thermodynamic performance of an absorption chiller employing the [emIm]DMP-H_2O working pair. Fig. 10 shows the effect of t_E on the COP of the system at t_G = 80 °C, t_C = 40 °C, and t_A = 35 °C. The results indicated that, at the same t_C and t_A, the COP of the [emIm]DMP-H_2O system is less than that of an aqueous solution of LiBr-H_2O but still greater than 0.7, whereas the t_G is less than that of the LiBr-H_2O system. Thus, [emIm]DMP-H_2O has the potential to be a new working pair for use in an absorption chiller driven by low-grade waste heat or hot water generated by a common solar collector.

http://dx.doi.org/10.5772/58982

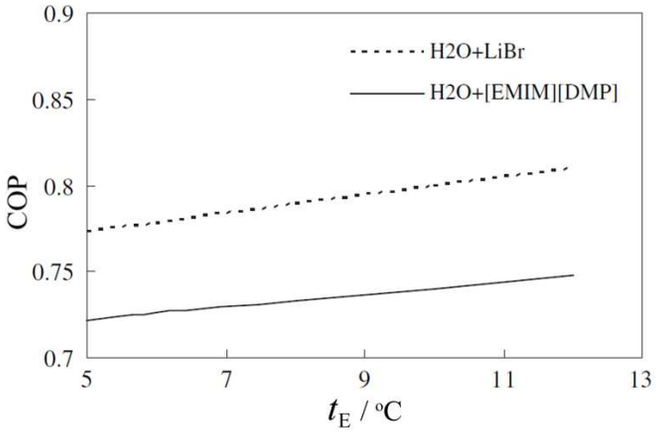


Figure 10. Effects of t_E on the COP of the [emIm]DMP-H_2O system.

2.4. Summary

All three of the working pairs described above possess good theoretical cycle characteristics that are better than those of H_2O-NH_3, but still slightly lower than those of LiBr-H_2O. Due to the advantages of the negligible vapor pressure of the absorbent, no corrosion, and no crystallization, these three working pairs can be applied in a wider range of operating conditions than H_2O-NH_3 or LiBr-H_2O. Therefore, it is expected that these three working pairs have enormous potential in industrial applications and strong possibilities for commercial development.

3. A new conceptual chemical absorption refrigeration working pair consisting of ammonia and a metal chloride-containing ionic liquid

3.1. The proposal

Adsorption refrigeration is a type of environmentally friendly refrigeration that has been studied for many years. The most commonly used working pairs in adsorption refrigeration systems are ammonia–activated carbon, methanol–activated carbon, water–zeolite, ammonia–calcium chloride, and methanol–calcium chloride. The first three are physical adsorption working pairs, and the last two are chemical adsorption working pairs. The following review begins with the NH_3-$CaCl_2$ system.

Calcium chloride reacts with ammonia to form coordination compounds:

$$\begin{aligned}
&CaCl_2 \cdot 8NH_3 + \Delta H_1 \leftrightarrow CaCl_2 \cdot 4NH_3 + 4NH_3 && \text{at } T_{e1}\\
&CaCl_2 \cdot 4NH_3 + \Delta H_2 \leftrightarrow CaCl_2 \cdot 2NH_3 + 2NH_3 && \text{at } T_{e2}\\
&CaCl_2 \cdot 2NH_3 + \Delta H_3 \leftrightarrow CaCl_2 + 2NH_3 && \text{at } T_{e3}
\end{aligned}$$

where ΔH_1~ΔH_3 are the enthalpies of the reaction, and T_{e1}~T_{e3} are the equilibrium temperatures. Benefiting from the reaction, the most impressive advantage of the NH_3-$CaCl_2$ system lies in its higher adsorption capacity compared to the others, while the main disadvantages are the low performances of heat and mass transfer and the phenomena of swelling and agglomeration in the process of adsorption [8]. Much effort has been spent attempting to overcome these defects. For example, Kai Wang et al. [9] proposed a new type of compound adsorbent composed of $CaCl_2$ and an expanded graphite adsorbent, which could mitigate the deterioration of the adsorption capacity that occurs in the long-term adsorption/desorption process. Using the compound adsorbent, Liwei Wang et al. [10] designed a multi-effect heat pipe-type adsorption refrigeration system, and a COP for their system of 0.39 was reported at a low t_E of -20 °C. Obviously, these improvements have little effect, and many other similar efforts [11] proved futile. The essence of all these failures can be attributed to the fact that the adsorbent is a solid. Except for $CaCl_2$, typical metal chlorides used as an ammonia adsorbent include $SrCl_2$, $LiCl_2$, and $ZnCl_2$, among others. If only the solid metal chlorides could be dissolved in ionic liquids, there would be no problem that could not be solved in the absorption or adsorption systems. Fortunately, a few ionic liquids containing metal chlorides have been synthesized, including [bmim]Zn_2Cl_5 [12], that offer high hydrothermal stability and negligible vapor pressure to perfectly meet the absorbent criteria for absorption refrigeration. Compared with a solid adsorbent or other ionic liquids, the advantage of the ionic liquid [bmim]Zn_2Cl_5 is self-evident. The chemical reaction between NH_3 and Zn^{2+} will largely enhance the solubility of NH_3 in the absorbent and reduce the pressure of vapor phase as well as in the NH_3-$CaCl_2$ system, and no defects in heat and mass transfer, swelling, or agglomeration are a problem. Some other metal cations such as Ni^{2+} [13], Cu^{2+} [14], and Fe^{3+} [15] were also found to dissolve in ionic liquids, and thus, a family of new conceptual chemical absorption refrigeration working pairs consisting of ammonia and metal chloride-containing ionic liquids seems ready to be developed.

3.2. VLE behavior of the binary system of NH_3-[bmim]Zn_2Cl_5

In order to reveal the promising latent application of NH_3-[bmim]Zn_2Cl_5 as a working pair in absorption refrigeration, the vapor pressure data of the binary system of [bmim]Zn_2Cl_5/NH_3 are urgently needed. In our previous work [16], VLE data for the binary system of NH_3-[bmim]Zn_2Cl_5 were measured and fitted using the modified UNIFAC (Dortmund) model.

3.2.1. Experimental data [16]

$100x_2$	p^{exp}/kPa	p^{cal}/kPa	$100x_2$	p^{exp}/kPa	p^{cal}/kPa	$100x_2$	p^{exp}/kPa	p^{cal}/kPa
T = 323.15 K			T = 383.15 K			86.04±0.04	1148.2	1148.5
85.78±0.04	67.4	65.6	91.34±0.05	699.6	704.5	87.34±0.05	1287.2	1188.0
86.84±0.04	77.4	77.0	92.39±0.05	829.7	828.8	89.05±0.05	1516.9	1517.5
87.76±0.05	87.7	88.6	93.67±0.06	1040.8	1029.9	90.58±0.06	1787.3	1787.5
88.92±0.05	103.5	106.7	T = 403.15 K			T = 483.15 K		
90.42±0.06	134.9	137.2	84.79±0.03	488.6	489.8	83.62±0.02	1081.2	1080.8

http://dx.doi.org/10.5772/58982

$100x_2$	p^{exp}/kPa	p^{cal}/kPa	$100x_2$	p^{exp}/kPa	p^{cal}/kPa	$100x_2$	p^{exp}/kPa	p^{cal}/kPa
91.76±0.06	170.8	174.2	85.90±0.04	544.9	546.5	84.83±0.03	1183.8	1182.7
92.77±0.07	210.6	210.8	86.86±0.05	602.3	603.5	85.88±0.04	1283.9	1284.4
93.99±0.08	285.6	269.6	88.08±0.05	687.5	689.4	87.21±0.05	1434.2	1435.1
	T = 343.15 K		89.68±0.06	829.9	832.7	88.94±0.05	1682.0	1682.2
85.65±0.03	119.6	117.8	91.11±0.06	1000.0	1003.1	90.49±0.06	1970.7	1972.3
86.72±0.04	137.4	136.5	92.19±0.07	1170.8	1170.1		T = 503.15 K	
87.63±0.05	155.8	155.6	93.51±0.07	1452.6	1439.7	83.48±0.02	1187.0	1185.3
88.80±0.05	183.4	184.8		T = 423.15 K		84.71±0.03	1294.9	1293.3
90.31±0.06	230.9	234.5	84.39±0.03	668.4	669.3	85.77±0.04	1400.7	1400.5
91.66±0.06	286.5	294.5	85.53±0.04	740.5	741.4	87.11±0.05	1558.8	1559.2
92.68±0.07	347.7	353.5	86.51±0.05	813.4	813.5	88.87±0.05	1816.5	1818.8
93.91±0.08	461.2	448.4	87.76±0.05	921.9	921.9		T = 523.15 K	
	T = 363.15 K		89.41±0.06	1100.9	1101.8	83.32±0.02	1300.6	1300.4
85.45±0.03	202.5	202.2	90.88±0.06	1313.0	1314.9	84.57±0.03	1414.3	1413.5
86.52±0.04	230.7	230.7	91.99±0.07	1523.0	1523.6	85.65±0.04	1525.2	1525.2
87.45±0.05	259.6	259.8	93.35±0.07	1859.8	1861.3	87.01±0.05	1688.7	1690.1
88.62±0.05	303.0	304.1		T = 443.15 K		88.80±0.05	1955.7	1957.8
90.15±0.06	375.1	378.9	84.08±0.03	821.5	821.4		T = 543.15 K	
91.52±0.06	463.8	468.7	85.24±0.04	905.7	905.1	83.11±0.02	1443.5	1443.6
92.55±0.07	555.1	557.1	86.25±0.05	989.4	988.8	84.38±0.03	1563.9	1563.5
93.81±0.08	711.8	699.5	87.53±0.05	1114.1	1114.0	85.48±0.04	1681.1	1681.5
	T = 383.15 K		89.21±0.06	1320.9	1320.6	86.87±0.04	1853.9	1854.1
85.15±0.03	327.4	325.3	90.71±0.06	1564.7	1564.5		T = 563.15 K	
86.25±0.04	368.5	366.5	91.85±0.07	1805.7	1802.7	83.02±0.02	1535.6	1535.8
87.19±0.05	410.7	408.2		T = 463.15 K		84.30±0.03	1661.9	1661.4
88.38±0.05	473.6	471.4	83.82±0.02	961.2	960.8	85.41±0.04	1784.8	1784.6
89.94±0.06	577.1	577.5	85.01±0.03	1055.2	1054.8	86.82±0.04	1964.6	1964.5

Table 2. The *P-T-x* data of binary solutions [bmim]Zn_2Cl_5 (1) + NH_3 (2)

The pressure-temperature-composition (*p-T-x*) data of the binary solutions [bmim]Zn_2Cl_5 (1) + NH_3 (2) with NH_3 mole fractions of x_2 = 0.83–0.94 at T = 323.15, 343.15, 363.15, 383.15, 403.15, 423.15, 443.15, 463.15, 483.15, 503.15, 523.15, 543.15, and 563.15 K are summarized in Table 2. The uncertainties in the NH_3 mole fraction in the binary solution, which can be due to the random and systematic errors in the experimental method and the calculation accuracy of the ammonia equation of state (EOS), are also presented in the table.

3.2.2. The modified UNIFAC (Dortmund) model [16]

Because of the non-volatilization of the ionic liquid [bmim]Zn_2Cl_5, the vapor phase of the binary system [bmim]Zn_2Cl_5 (1) + NH_3 (2) consists only of NH_3, and the total pressure p of the binary solution can be given by [17],

$$p = x_2\gamma_2 P_2^{S'} \exp\left(\frac{(V_2^L - B_2)(p - P_2^{S'})}{RT}\right) \tag{1}$$

where x_2 is the mole fraction of NH_3 in the binary solution, γ_2 is the activity coefficient of NH_3, V_2^L is the liquid mole volume of NH_3, B_2 is the second virial coefficient in the ammonia EOS, and $P_2^{S'}$ is the vapor pressure of pure NH_3, When the temperature T is below the T_C, $P_2^{S'}$ is equal to the saturation vapor pressure, P^S, which can be calculated by [18],

$$\ln P_2^{S'} = \frac{1}{T_r - 0.101947}\left(-4.2522T_r^2 + 7.929445T_r^3 + 0.3807783T_r^7 - 4.039557\right) \tag{2}$$

where T_r is the ratio of the solution temperature T and T_C, When the temperature T is higher than the T_C, the $P_2^{S'}$ is defined as the pure NH_3 pressure at T and the critical mole fraction V_C, which can be calculated by the RK type EOS as follows [19]:

$$P_2^{S'} = \frac{RT}{V_C - b} - \frac{a(T)}{V_C(V_C + b)} \tag{3}$$

$$a(T) = 0.42748\alpha(T)R^2T_C^{\,2}/P_C \tag{4}$$

$$b = 0.08664RT_C/P_C \tag{5}$$

where the temperature dependent term $\alpha(T)$ can be written by:

$$\alpha(T) = \sum_{k=0}^{2}\beta_k\left(1/T_r - T_r\right)^k \tag{6}$$

The EOS constants for NH_3 β_k and the critical parameters T_C, V_C, and P_C are given in Table 3.

β_0	β_1	β_2	T_C / K	P_C / kPa	V_C / m^3mol^{-1}
1.00027	0.45689	-0.05772	406.15	11424	0.00427

Table 3. EOS constants and critical parameters for NH_3

In the UNIFAC model, the excess Gibbs free energy is composed of two contributing parts, the combinatorial part and the residual part, and the activity coefficient γ_i can be given as follows:

$$\ln \gamma_i = \ln \gamma_i^C + \ln \gamma_i^R \tag{7}$$

where γ_i^C is the combinatorial activity coefficient and γ_i^R is the residual activity coefficient.

The combinatorial activity coefficient γ_i^C describes the repulsive interaction attributed to the molecular size and shape, which can be calculated by:

$$\ln \gamma_i^C = \ln \frac{\varphi_i}{x_i} + \frac{Z}{2} q_i \ln \frac{\theta_i}{\varphi_i} + l_i - \frac{\varphi_i}{x_i} \sum_j x_j l_j \tag{8}$$

$$l_i = \frac{Z}{2}(r_i - q_i) - (r_i - 1) \tag{9}$$

$$\theta_i = q_i x_i / \sum_j q_j x_j \tag{10}$$

$$\varphi_i = r_i x_i / \sum_j r_j x_j \tag{11}$$

$$q_i = \sum \nu_k^{(i)} Q_k \tag{12}$$

$$r_i = \sum \nu_k^{(i)} R_k \tag{13}$$

where Z is normally set to 10, $v_k^{(i)}$ is the number of group k in component i, and R_k and Q_k are the volume and surface parameters of the group k, respectively. The values of R_k and Q_k for the group used in our experiment are listed in Table 4.

	[bmim]$^+$	**Zn^{2+}**	**Cl^-**	**NH_3**
R_k	6.0334 [20]	3.0 [21]	0.6560 [20]	0.8239 [22]
Q_k	4.7910 [20]	3.0 [21]	0.6730 [20]	0.7780 [22]

Table 4. Volume parameters R_k and surface parameters Q_k

The residual activity coefficient γ_i^R accounts for the intermolecular forces resulting from the corresponding group interaction, which is described as the summation of the group activity coefficient Γ for group k of component i,

$$\ln \gamma_i^R = \sum_k^N \nu_k^{(i)} (\ln \Gamma_k - \ln \Gamma_k^{(i)}) \tag{14}$$

where Γ_k and $\Gamma_k^{(i)}$ are the activity coefficients for group k in binary solution and in the component i, respectively, and can be described as:

$$\ln \Gamma_k = Q_k[1 - \ln(\sum_{m=1}^{N} \theta_m \phi_{mk}) - \sum_{m=1}^{N} (\frac{\theta_m \phi_{km}}{\sum_{n=1}^{N} \theta_n \phi_{nm}})] \tag{15}$$

$$\theta_m = Q_m X_m / \sum_{n=1}^{N} Q_n X_n \tag{16}$$

$$X_m = \sum_{j=1}^{M} \nu_m^{(j)} x_j / \sum_{j=1}^{M} \sum_{n=1}^{N} \nu_n^{(j)} x_j \tag{17}$$

Eqs. 15–17 can also be used to calculate $\ln\Gamma_k^{(i)}$, except that the group composition variable X_m is now the group fraction of group k in component i. For the modified UNIFAC (Dortmund) model, the group interaction parameters between groups n and m, $\varphi_{n,m}$, is described as:

$$\phi_{n,m} = \exp(-\frac{a_{nm} T^2 + b_{nm} T + c_{nm}}{T}) \tag{18}$$

where a_{nm} (K^{-1}), b_{nm}, and c_{nm} (K) are the adjustable interaction parameters for correlating the experimental vapor pressure data. The corresponding correlation results are listed in Table 5.

n	m	a_{nm}/K^{-1}	b_{nm}	c_{nm}/K
NH_3	$[bmim]^+$	0.00617	-1.9768	-378.1920
NH_3	Zn^{2+}	-0.02754	2.7884	1119.6973
NH_3	Cl^-	0.03904	-39.2835	11459.2768
$[bmim]^+$	NH_3	-0.00915	-2.7566	2059.6872
$[bmim]^+$	Zn^{2+}	-0.01720	-12.6476	5508.8668
$[bmim]^+$	Cl^-	22.62142	-82.6723	-5307.7598
Zn^{2+}	NH_3	-0.00911	-3.0401	2070.4982
Zn^{2+}	$[bmim]^+$	-0.02991	-6.8487	12385.2753
Zn^{2+}	Cl^-	16.45937	66.7508	-2708.8868
Cl^-	NH_3	-0.00281	-1.6807	-548.2453
Cl^-	$[bmim]^+$	0.09208	313.3495	-86.4292
Cl^-	Zn^{2+}	0.19296	59.8376	-5434.4813

Table 5. Adjustable interaction parameters for UNIFAC model

http://dx.doi.org/10.5772/58982

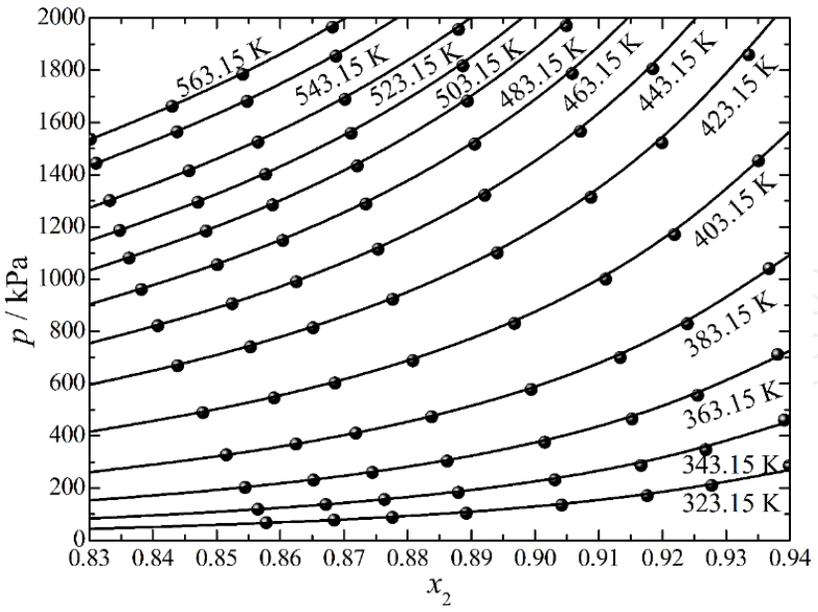


Figure 11. *P-T-x* phase diagrams (Lines: calculated with the UNIFAC model. Symbols: experimental data) [16].

The *P-T-x* phase diagrams with symbols for experimental data and lines for the UNIFAC model calculations are shown in Fig. 11. It can be seen from the figure that with an increase in the NH_3 mole fraction, the vapor pressure also increases, and the rising trend becomes increasingly more obvious. With an increase in the binary solution temperature, the vapor pressure increases rapidly. When the temperature is below the T_C, the rate of increase becomes more rapid, but when the temperature is higher than the T_C of NH_3, the rate of increase tends to slow and the vapor pressure even declines slightly.

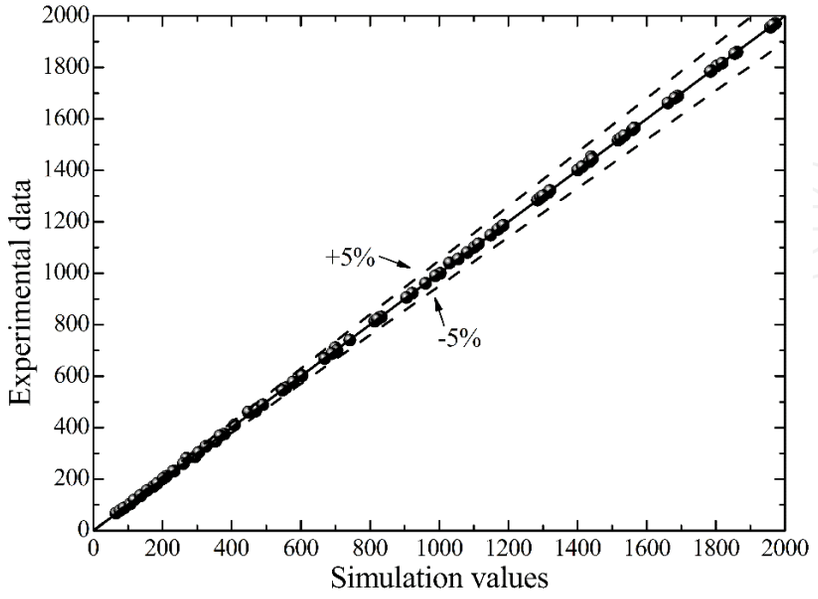


Figure 12. Comparison of experimental data and the UNIFAC model calculations [16].

A comparison of the experimental data and the UNIFAC model calculations is shown in Fig. 12. All deviations are below 5.0% and are mainly produced by the uncertainties in the volumes of the high pressure vessel (0.7%) and liquid phase of binary system (1.1%), the weights of [bmim]Zn_2Cl_5 (0.01%) and NH_3 (0.05%), the temperature distribution in the high pressure vessel (0.7%), EOS calculation accuracy (1.2%), and the fitting uncertainty (1.6%). Based on the above uncertainties, the total uncertainty of the measurements is estimated to be within 4.3%.

3.2.3. Comparison with normal ionic liquids and $ZnCl_2$

Fig. 13 compares the vapor pressures of [bmim]Zn_2Cl_5/NH_3 solutions with x_2 = 0.9507 and 0.9231 to those of $ZnCl_2$ 6NH_3 [23] at T = 330–420 K. When x_2 = 0.9507, the NH_3 mass fraction of the binary solution is equal to the NH_3 mass fraction in $ZnCl_2$ 6NH_3, and when x_2 = 0.9231, the mole ratio of NH_3 and Zn^{2+} is 6, which is equal to that in $ZnCl_2$ 6NH_3. From Fig. 13, the vapor pressures of NH_3 in [bmim]Zn_2Cl_5 with x_2 = 0.9507 and 0.9231 are 2–3 times higher than that of $ZnCl_2$ 6NH_3, which can be attributed to the effects of the ionic liquid [bmim]Cl on the complexation reaction production of NH_3 and Zn^{2+} ions.

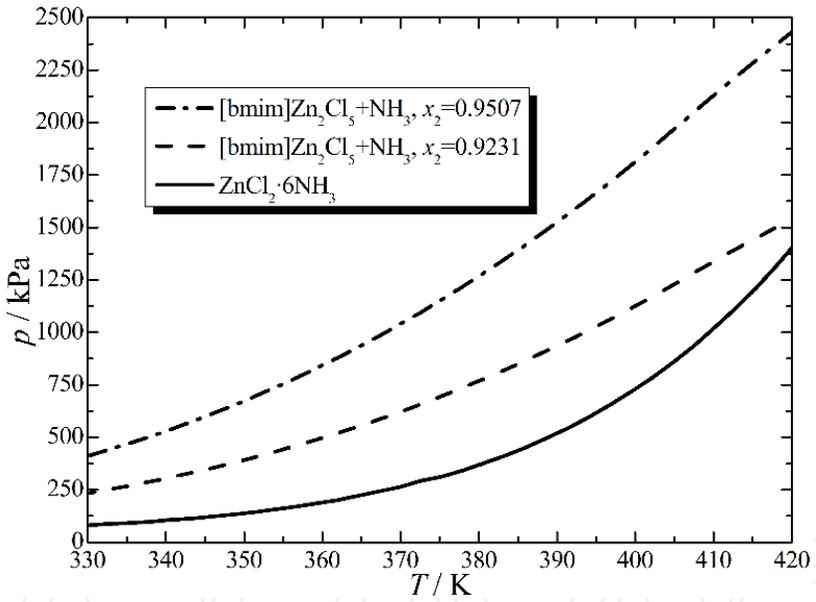


Figure 13. Comparison of vapor pressures of NH_3-[bmim]Zn_2Cl_5 solution and $ZnCl_2$ 6NH_3 [16].

Fig. 14 compares the vapor pressure of the NH_3-[bmim]Zn_2Cl_5 solution and ammonia solutions containing ionic liquids [19] [emim][Ac], [emim][SCN], [emim][$EtOSO_3$], and [DMEA][Ac] at T = 348 K and x_2 = 0–1. From Fig. 14, the vapor pressure of NH_3 in [bmim]Zn_2Cl_5 is one order of magnitude smaller than that in normal ionic liquids at x_2 = 0–0.95, which means that the complexion reaction of NH_3 and Zn^{2+} ions can largely reduce the vapor pressure of NH_3 in the ionic liquid and largely enhance the solubility of NH_3 in the ionic liquid.

Based on the results in Figs. 13 and 14, the absorption characteristics of [bmim]Zn_2Cl_5 are much better than those of normal ionic liquids but slightly lower than those of $ZnCl_2$. Additionally,

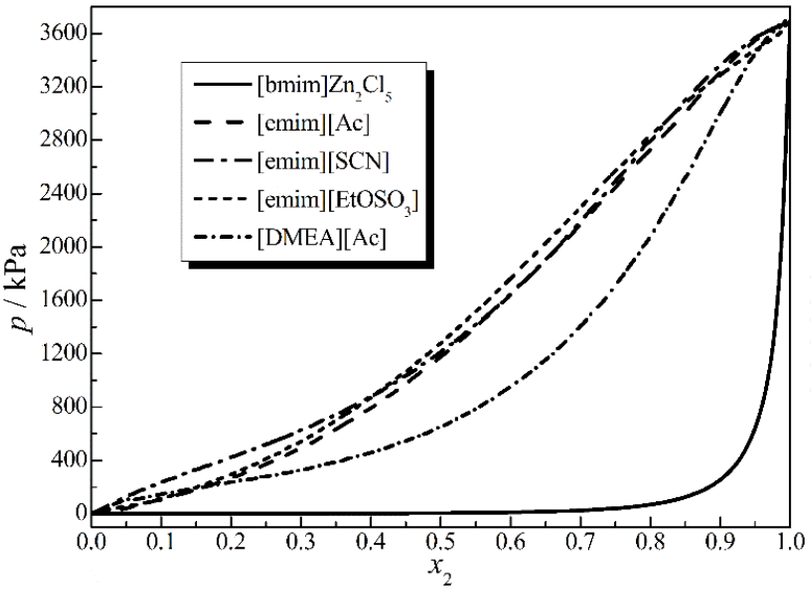


Figure 14. Comparison of vapor pressures of [bmim]Zn_2Cl_5/NH_3 solution and ammonia solutions containing the ionic liquids [emim][Ac], [emim][SCN], [emim][$EtOSO_3$] and [DMEA][Ac] [16].

the liquid form of [bmim]Zn_2Cl_5 offers a major advantage over $ZnCl_2$, which will completely resolve the abovementioned limitations to improve the cycle performance for $ZnCl_2$/NH_3 adsorption refrigeration. Therefore, working pairs of NH_3-[bmim]Zn_2Cl_5 have good latent application potential in absorption refrigerator and heat pump operation.

3.3. Heat capacities and excess enthalpies of the NH_3-[bmim]Zn_2Cl_5 system

In order to investigate the cycle characteristics of [bmim]Zn_2Cl_5/NH_3 absorption refrigeration, data for the heat capacities of [bmim]Zn_2Cl_5 and excess enthalpies of [bmim]Zn_2Cl_5/NH_3 are urgently needed. In our previous work, the heat capacities of [bmim]Zn_2Cl_5 for T = 210.15–383.15 K were obtained by differential scanning calorimetry (DSC), and the excess enthalpies of [bmim]Zn_2Cl_5/NH_3 at various ammonia mole fractions for T = 288.15–333.15 K were measured experimentally. The data for excess enthalpies were fit by a five-parameter NRTL model. Based on the heat capacity of [bmim]Zn_2Cl_5 and the excess enthalpy of [bmim]Zn_2Cl_5/NH_3, the enthalpies of [bmim]Zn_2Cl_5/NH_3 solution at x_1 = 0–1 for T = 273.15–343.15 K were calculated.

3.3.1. Heat capacities of [bmim]Zn_2Cl_5

Fig. 15 shows the result of TG scanning for [bmim]Zn_2Cl_5, which was determined using a TGA/SDT instrument. Onset of a 2.5% weight loss in a nitrogen atmosphere occurs at 676.15 K, and approximately 40% of the mass is gone by 774.15 K, which is a typical volatilization temperature for imidazolium salts. Continued heating of [bmim]Zn_2Cl_5 eventually results in a constant weight near 1043.15 K, with a residual weight of 36.4%. These results indicate that [bmim]Zn_2Cl_5 possesses high thermal stability at T < 673.15 K.

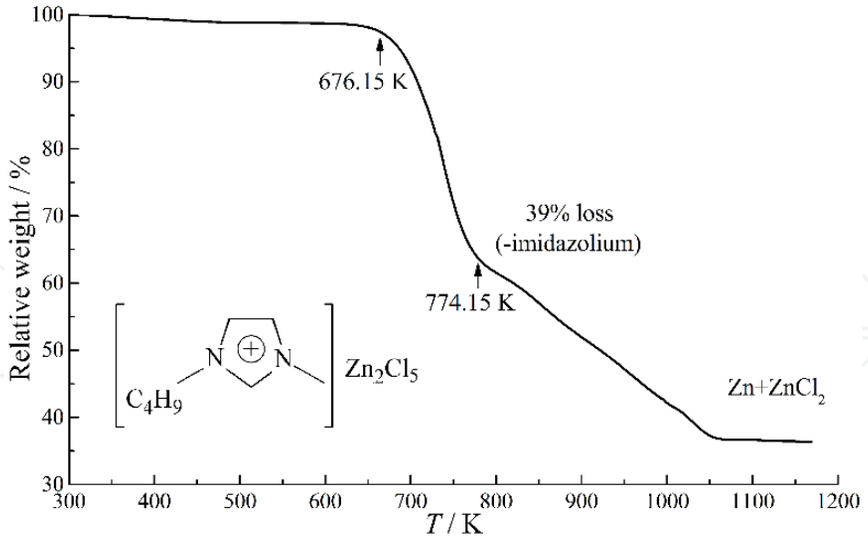


Figure 15. Thermogravimetric (TG) scan results for [bmim]Zn_2Cl_5.

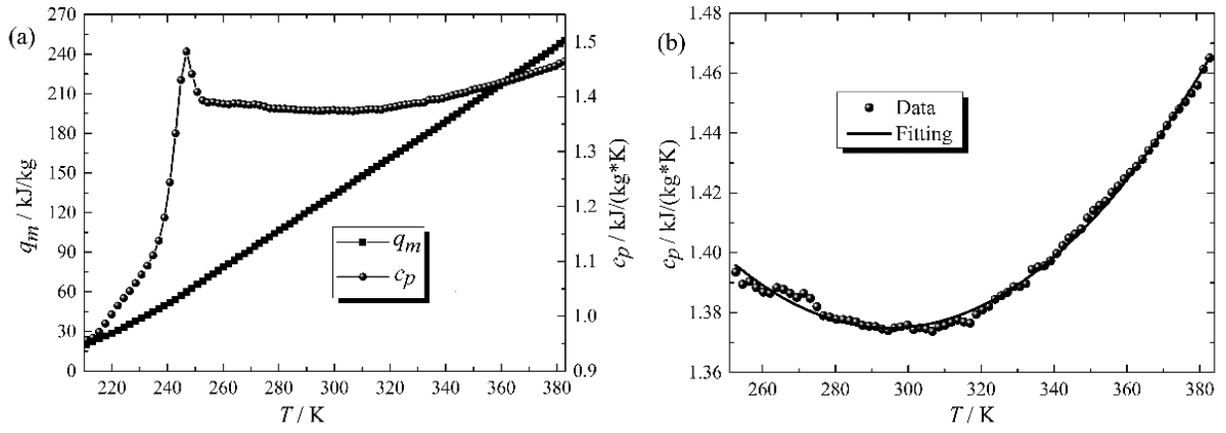


Figure 16. DSC scanning results for [bmim]Zn_2Cl_5: (a) variations in heat flow, q_m, and specific heat capacity, c_p, along with the temperature of [bmim]Zn_2Cl_5; (b) c_p-T diagram of [bmim]Zn_2Cl_5 for T = 243.15–383.15 K.

Fig. 16(a) shows the variation in the specific heat flow, q_m, and the specific heat capacity, c_p, along with temperature variations for [bmim]Zn_2Cl_5. The specific heat flow increases with an increase in temperature. The rate of increase of the specific heat flow rises at T < 243.15 K, and the variation in the rate of increase of the specific heat flow is minor for T > 243.15 K. The specific heat capacity increases with an increase in the [bmim]Zn_2Cl_5 temperature at T < 243.15 K, and the rate of increase also increases. The specific heat capacity presents an increasing trend after a decline for T > 243.15 K. These results indicate that the melting temperature of [bmim]Zn_2Cl_5 is near 243.15 K. By careful observation, it is found that variations in the specific heat capacity with T > 251.15 K can be well fitted by the following quadratic equation:

$$c_p = 2.39327\text{-}0.00691T + 0.000011767\,T^2 \tag{19}$$

Fig. 16(b) shows the c_p-T diagram for T = 243.15–383.15 K. The symbols represent the experimental data, and the lines represent the calculated conic curve. It can be seen that variation in the specific heat capacity with temperature is accurately described by the quadratic curve.

3.3.2. Experimental data for excess enthalpy of NH_3-[bmim]Zn_2Cl_5

Temperature-component-molar excess enthalpy (T-x-H^E) data for the binary systems [bmim]Zn_2Cl_5 (2) + NH_3 (1) at ammonia mole fractions of x_1 = 0.60–0.95 and T = 288.15, 303.15, 318.15, and 333.15 K are summarized in Table 6. Uncertainties in the temperature, ammonia mole fraction, and molar excess enthalpy are also presented in the table. The uncertainties are due to random errors as well as systematic errors for the experimental apparatus and the calculation accuracy of the UNIFAC model for the VLE of NH_3/[bmim]Zn_2Cl_5. With an increase in the ammonia mole fraction, x_1, the molar excess enthalpy presents an increasing trend after an initial decline.

T/K	x_2	H^E/*J/mol*	*T/K*	x_2	H^E/*J/mol*
288.15	0.617	-6052	318.15	0.631	-6237
288.15	0.709	-6446	318.15	0.725	-6795
288.15	0.819	-6385	318.15	0.796	-6825
288.15	0.873	-6007	318.15	0.877	-6301
288.15	0.935	-4778	318.15	0.929	-5282
303.15	0.614	-6102	333.15	0.622	-6233
303.15	0.718	-6657	333.15	0.698	-6851
303.15	0.782	-6665	333.15	0.773	-6870
303.15	0.866	-6242	333.15	0.854	-6638
303.15	0.947	-4393	333.15	0.931	-5412

Table 6. Mole excess enthalpy of binary systems [bmim]Zn_2Cl_5 (1) + NH_3 (2).

3.3.3. NRTL model

Based on the local composition representation of the excess Gibbs energy, G^E, Renon and Prausnitz [24] proposed the NRTL model. The G^E for the NRTL model can be described by:

$$\frac{G^E}{RT} = x_1 x_2 \left(\frac{\tau_{21} G_{21}}{x_1 + x_2 G_{21}} + \frac{\tau_{12} G_{12}}{x_2 + x_1 G_{12}} \right) \tag{20}$$

$$\tau_{12} = \frac{g_{12} - g_{22}}{RT}, \tau_{21} = \frac{g_{21} - g_{11}}{RT} \tag{21}$$

$$G_{12} = \exp\left(-\alpha\tau_{12}\right), G_{21} = \exp\left(-\alpha\tau_{21}\right) \tag{22}$$

where g_{ij} and g_{jj} are the interaction energy between ij and jj component pairs, respectively, and α is the non-random parameter. The relationship between G^E and the activity coefficient is given by:

$$G^E = RT\sum_i \ln\gamma_i + \sum_{k\neq i}\left(\frac{\partial G^E}{\partial x_i}\right)_{T,P,x_{j\neq ik}} \tag{23}$$

Therefore, the activity coefficients of components 1 and 2 in a binary mixture can be written as:

$$\ln\gamma_1 = x_2^2\left[\tau_{21}\left(\frac{G_{21}}{x_1 + x_2G_{21}}\right)^2 + \left(\frac{\tau_{12}G_{12}}{(x_2 + x_1G_{12})^2}\right)\right] \tag{24}$$

$$\ln\gamma_2 = x_1^2\left[\tau_{12}\left(\frac{G_{12}}{x_2 + x_1G_{12}}\right)^2 + \left(\frac{\tau_{21}G_{21}}{(x_1 + x_2G_{21})^2}\right)\right] \tag{25}$$

The definition of the activity coefficient for ammonia, γ_1, is presented in our previous work [16]. For the NRTL model, the interaction energy between the ij and jj component pairs are defined as:

$$g_{12} - g_{22} = A_1 + B_1T \tag{26}$$

$$g_{21} - g_{11} = A_2 + B_2T \tag{27}$$

The Gibbs-Helmholtz equation for excess enthalpy is:

$$-\frac{H^E}{T^2} = \left[\frac{\partial\left(G^E/T\right)}{\partial T}\right]_{P,x} \tag{28}$$

For the five-parameter NRTL model, the excess enthalpy can be calculated by:

$$H^E = -x_1x_2\left\{\frac{A_2G_{21}\left[x_1\tau_{21}\left(\alpha\tau_{21} - 1\right) - x_2G_{21}\right]}{\left(x_1 + x_2G_{21}\right)^2} + \frac{A_1G_{12}\left[x_2\tau_{12}\left(\alpha\tau_{12} - 1\right) - x_1G_{12}\right]}{\left(x_2 + x_1G_{12}\right)^2}\right\} \tag{29}$$

The correlation results are shown in Table 7.

α	A_1/Jmol^{-1}	B_1/Jmol^{-1}K^{-1}	A_2/Jmol^{-1}	B_2/Jmol^{-1}K^{-1}
0.1043	14062.6306	419.6197	-164.3040	-256.9565

Table 7. Binary parameters and non-random parameters for NRTL model

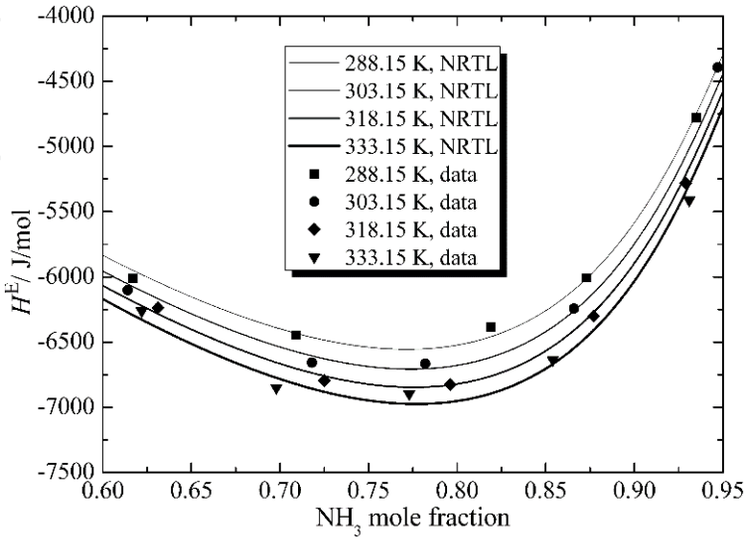


Figure 17. T-x-H^E diagram of [bmim]Zn_2Cl_5/NH_3 for T = 288.15–333.15 K.

Fig. 17 shows the T-x-H^E diagram for the binary system of [bmim]Zn_2Cl_5/NH_3 at T = 288.15–333.15 K. The symbols represent the experimental data, and the lines represent the calculations from the NRTL model. From Fig. 17, with an increase in the NH_3 mole fraction, the excess enthalpy shows an increasing trend after a decline. There are minimum excess enthalpies for each temperature: -6555.7, -6707.1, -6846.3, and -6974.7) J/mol appear at x_1 = 0.772, 0.774, 0.776, and 0.777 for T = 288.15, 303.15, 318.15, and 333.15 K, respectively.

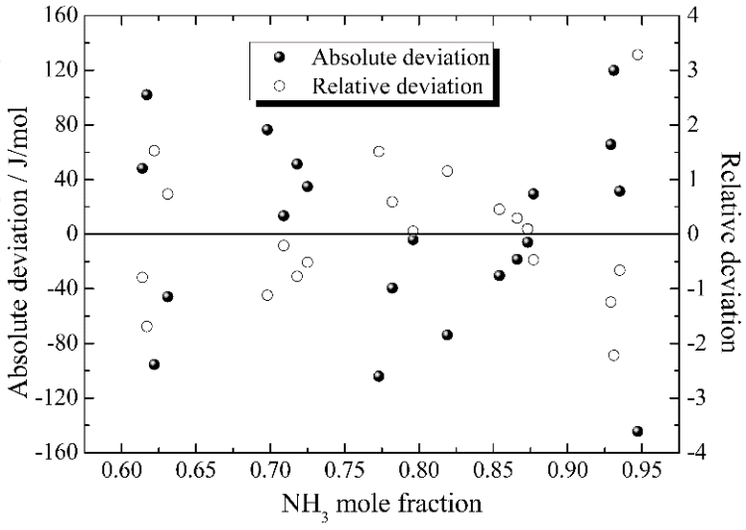


Figure 18. Absolute deviations and relative deviations with the NRTL model.

Fig. 18 shows the absolute deviations and relative deviations between the experimental data and the values predicted by the NRTL model for excess enthalpy data. The results indicate that all deviations for excess enthalpy data are less than 3.9%. The measurement deviations are mainly produced by the uncertainties in volumes of the high pressure vessels (0.5%), the little tank (0.5%) and the liquid phase of binary system (0.2%); the weights of [bmim]Zn_2Cl_5 (0.01%), NH_3 (0.05%) and water (0.01%); temperature distributions in the water bath (1.4%) and the bath container (1.2%); and the UNIFAC calculation accuracies (0.9%). Based on the above uncertainties, the total uncertainty of measurement is estimated to be less than 4.8 %.

3.3.4. Enthalpy of [bmim]Zn_2Cl_5/NH_3 solution

The enthalpy of a solution of [bmim]Zn_2Cl_5/NH_3 at T and a given NH_3 mass fraction ω_1 can be calculated by:

$$h = (1-\omega_1)h_1 + \omega_1 h_2 + h^{\mathrm{E}} \tag{30}$$

The enthalpy of [bmim]Zn_2Cl_5, h_1, can be calculated by:

$$h_1 = \int_{T_0}^{T} c_p \, dT \tag{31}$$

where c_p is the specific heat capacity of [bmim]Zn_2Cl_5, which can be calculated using Eq. (1), and T_0 is defined as 273.15 K. The enthalpy of NH_3 can be calculated by [19]:

$$h_2 = \sum_{i=0}^{6} a_i \left(T - 273.15\right)^i \tag{32}$$

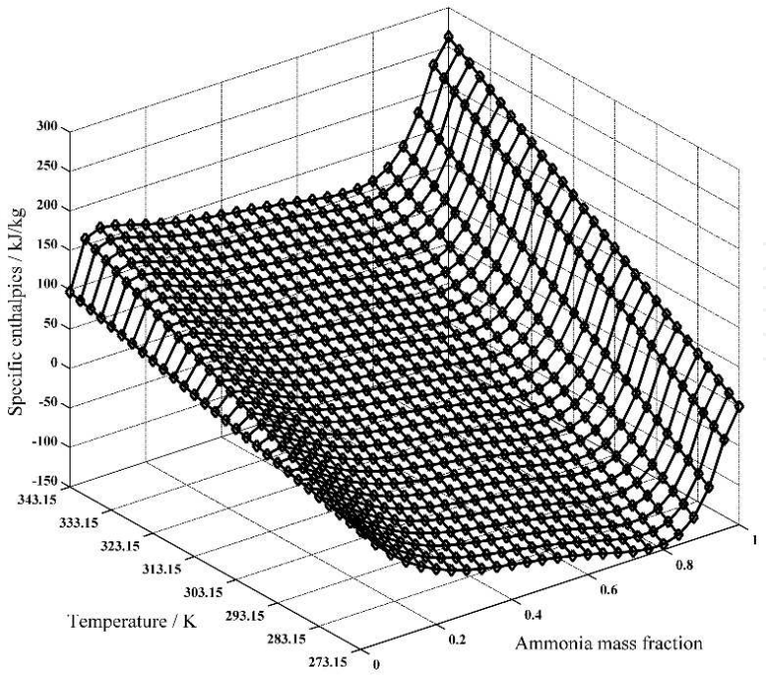


Figure 19. Calculations for enthalpies of [bmim]Zn_2Cl_5/NH_3 solution at x_1 = 0–1 for T = 273.15–343.15 K.

Fig. 19 shows the calculated enthalpies for [bmim]Zn_2Cl_5/NH_3 solution at ω_1 = 0–1 and T = 273.15–343.15 K. Based on the VLE properties and the enthalpies of [bmim]Zn_2Cl_5/NH_3 solutions, the thermodynamic performances of the [bmim]Zn_2Cl_5/NH_3 absorption system can be investigated.

3.4. Thermodynamic analysis of an absorption system using NH_3-[bmim]Zn_2Cl_5 as the working pair [25]

In our previous work, the modified UNIFAC model was used to describe the VLE properties of [bmim]Zn_2Cl_5/NH_3 [16] and the NRTL model was used to predict the excess enthalpic properties of [bmim]Zn_2Cl_5/NH_3. Based on a single-effect absorption refrigeration model, the thermodynamic performance of the [bmim]Zn_2Cl_5/NH_3 absorption system was simulated and compared with that of the $NaSCN/NH_3$ adsorption system. The coefficients of performance for cooling (COP) and heating (COP^*) and circulation ratios under the condition of a subzero evaporating temperature were calculated and analyzed.

3.4.1. System description and simulation

Fig. 20 shows a schematic diagram of the single effect absorption system. The main system is composed of the generator (G), the absorber (A), the condenser (C), the evaporator (E), the regenerator (R), the valves (V), and the solution pump (P). In Fig. 20, the status point numbers are given, and the fluids at each point are marked: *i* denotes the [bmim]Zn_2Cl_5/NH_3 solution from the absorber with a high NH_3 mass fraction, *ii* denotes the [bmim]Zn_2Cl_5/NH_3 solution from the generator with a low NH_3 mass fraction, and *iii* denotes the refrigerant NH_3. The symbols q_E, q_C, q_A, and q_G represent the heat flow of the evaporator, the condenser, the absorber, and the generator, respectively.

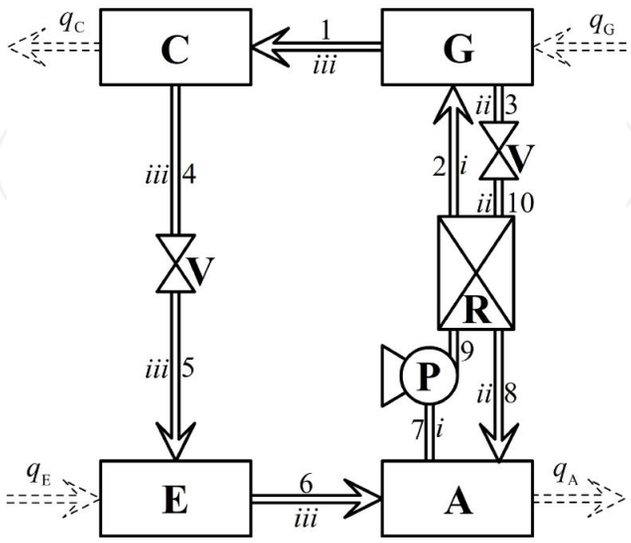


Figure 20. Schematic diagram of the single effect absorption system [25].

In order to simulate the thermodynamic performance of an absorption system using [bmim]Zn_2Cl_5/NH_3 as a working pair, several assumptions were made as follows [25]:

1. The simulation is conducted under steady state;
2. The vapor pressure losses are neglected, the pressure of the evaporator is equal to that of the absorber, and the pressure of the condenser is equal to that of the generator;
3. The refrigerant flowing out of the condenser is in a saturated liquid state, and the refrigerant flowing out of the evaporator is in a saturated gas state;
4. The heat recovery rate of the regenerator is set to 0.80 [26]; and
5. The thermal losses and pumping work are negligible.

The mass and energy conservation equations for the evaporator are given by:

$$m_5 = m_6 \tag{33}$$

$$q_{\mathrm{E}} = m_6 h_6 - m_5 h_5 \tag{34}$$

The mass and energy conservation equations for the condenser are given by:

$$m_1 = m_4 \tag{35}$$

$$q_{\mathrm{C}} = m_1 h_1 - m_4 h_4 \tag{36}$$

For the absorber, the mass conservation equation of the solution, the mass conservation equation of IL, and the energy conservation equation are given by:

$$m_7 = m_6 + m_8 \tag{37}$$

$$m_7(1-\omega_7) = m_6 + m_8(1-\omega_8) \tag{38}$$

$$q_{\mathrm{A}} = m_6 h_6 + m_8 h_8 - m_7 h_7 \tag{39}$$

For the generator, the mass conservation equation of the solution, the mass conservation equation of IL, and the energy conservation equation are given by:

$$m_2 = m_1 + m_3 \tag{40}$$

$$m_2(1-\omega_2) = m_1 + m_3(1-\omega_3) \tag{41}$$

$$q_G = m_1 h_1 + m_3 h_3 - m_2 h_2 \tag{42}$$

For the regenerator, the energy conservation equation is given by:

$$m_2(h_2 - h_9) = m_3(h_{10} - h_8) \tag{43}$$

Based on the above assumptions and the conservation equations for mass and energy conservation, the heat flow values of q_G, q_C, q_E, and q_A; mass flow values of m_2 and m_3; and mass fractions of ω_2 and ω_3, can be calculated. The circulation ratio (f) is calculated by:

$$f = \frac{m_3}{m_1} = \frac{1-\omega_3}{\omega_2 - \omega_3} \tag{44}$$

The COP for cooling is defined by:

$$COP = \frac{q_E}{q_G} \tag{45}$$

The exergy efficiency (η_{ex}) for cooling is given by:

$$\eta_{ex} = \frac{q_E\left(\frac{T_0}{T_E} - 1\right)}{q_G\left(1 - \frac{T_0}{T_G}\right)} \tag{46}$$

The COP* for heating is defined as:

$$COP^* = \frac{q_A + q_C}{q_G} = 1 + \frac{q_E}{q_G} \tag{47}$$

The exergy efficiency for cooling (η^*_{ex}) is given by:

$$\eta^*_{ex} = \frac{q_C\left(1 - \frac{T_0}{T_C}\right) + q_A\left(1 - \frac{T_0}{T_A}\right)}{q_G\left(1 - \frac{T_0}{T_G}\right)} \tag{48}$$

3.4.2. Results and discussion

Fig. 22 shows variations in the COP and η_{ex} of [bmim]Zn_2Cl_5/NH_3 absorption refrigeration with variations in t_A and t_C at a t_G = 90 °C and t_E = -10 °C. These results show that both the COP and η_{ex} decline with increases in t_A and t_C. This is because increases in t_A and t_C lead to a decrease in the mass fraction of solution from the absorber (ω_2) and an increase in the mass fraction of solution from the generator (ω_3). These changes in both ω_2 and ω_3 result in a decrease of q_E. The slopes of both the COP and η_{ex} curves are less steep when t_A and t_C are lower, and as t_A and t_C continue to increase, the slopes become increasingly steep. This can be explained by the fact that,with the continuous increases in t_A and t_C, the difference between ω_2 and ω_3 continues to become smaller. By comparison, the thermal performance of the [bmim]Zn_2Cl_5/NH_3 system is better than that of the NaSCN/NH_3 system when t_A and t_C are low. However, when t_A and t_C are high, the thermal performance of the NaSCN/NH_3 system is better than that of the [bmim]Zn_2Cl_5/NH_3 system, and the upper operating limit of t_A and t_C for NaSCN/NH_3 is higher than that for the [bmim]Zn_2Cl_5/NH_3 system. This can also be explained by the properties of NH_3 solubility in [bmim]Zn_2Cl_5 and NaSCN. The higher solubility of NH_3 in [bmim]Zn_2Cl_5 ensures that the [bmim]Zn_2Cl_5/NH_3 system possesses better thermal performance than the NaSCN/NH_3 system with operating conditions of low t_A and t_C. The stronger combination of NH_3 and [bmim]Zn_2Cl_5 demonstrates that the upper operating limit of t_A and t_C for the [bmim]Zn_2Cl_5/NH_3 system are lower than those of the NaSCN/NH_3 system.

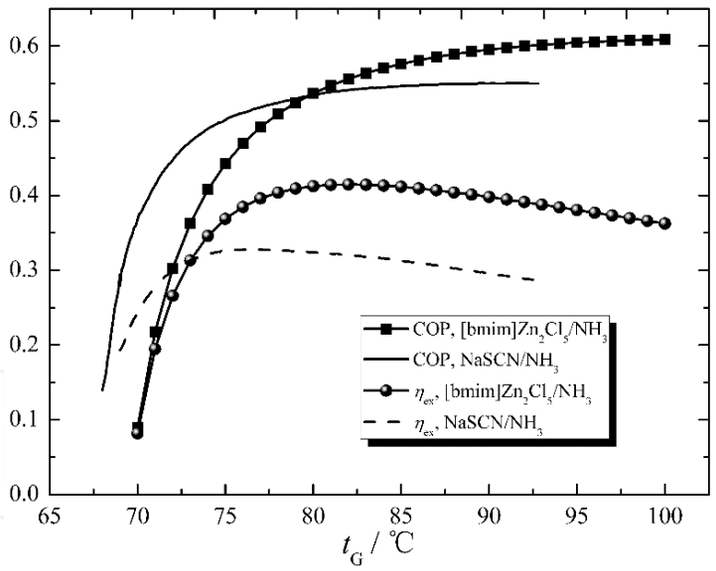


Figure 21. Variations in the COP and η_{ex} of [bmim]Zn_2Cl_5/NH_3 absorption refrigeration with changes in T_G for t_A = t_C = 25 °C and t_E= -10 °C [25].

Fig. 23 shows the effects of t_G on the COP for t_G = 110–230 °C with t_A = t_C = 35 °C and t_E= -10 °C, -20 °C, -30 °C, or -40 °C. With an increase in t_G, the COP presents a trend of first increasing and the decreasing. The reason for this trend is that the increase in t_G has both positive and negative effects on the COP. The positive and negative effects are the same as indicated by the analysis of the trend in COP shown in Fig. 2. When t_G is lower, the positive effect is predominant, and

http://dx.doi.org/10.5772/58982

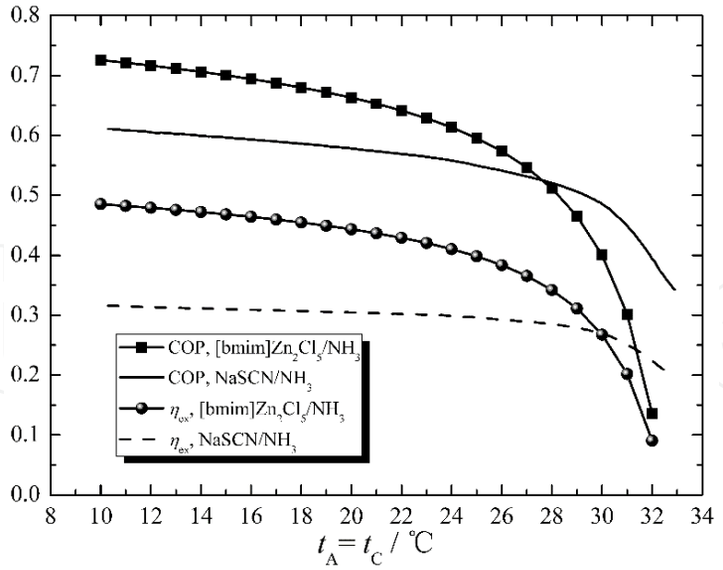


Figure 22. Variations in the COP and η_{ex} of [bmim]Zn_2Cl_5/NH_3 absorption refrigeration with varying t_A and t_C for t_G = 90 °C and t_E = -10 °C [25].

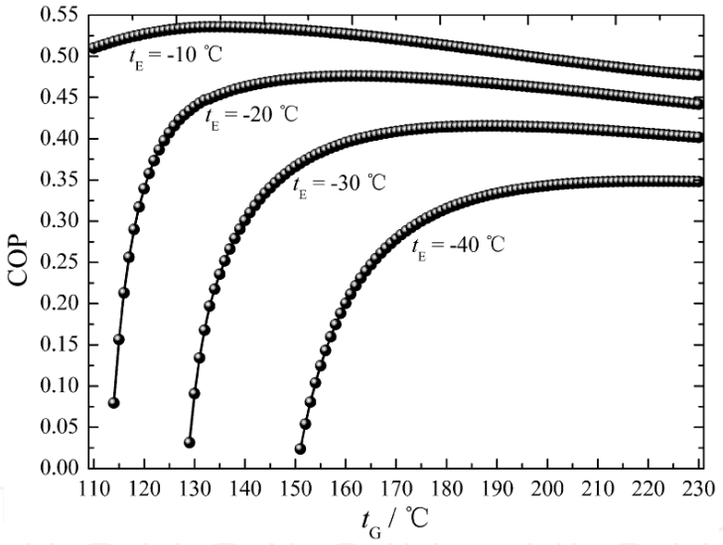


Figure 23. Effects of T_G on the COP for t_G = 110–230 °C, t_A = t_C = 35 °C and t_E= -10 °C, -20 °C, -30 °C, or -40 °C [25].

the COP increases with an increase in t_G. With a further increase in t_G, the negative effect is gradually enhanced, and the rate at which the COP increases is continually reduced until it finally becomes negative. When t_G is higher, the negative effect is predominant, and the COP decreases with an increase in t_G. For t_E= -10 °C, -20 °C, -30 °C, and -40 °C, the maximum COPs for the [bmim]Zn_2Cl_5/NH_3 system of 0.54, 0.48, 0.42, and 0.35 appear at t_G =133 °C, 161 °C, 188 °C, and 225 °C, respectively. When t_E = -10 °C and -20 °C, the maximum COPs for the NaSCN/NH_3 system occurs at t_G = 81 °C and 98 °C, respectively [27]. These results indicate that the required temperature of the heat source for the [bmim]Zn_2Cl_5/NH_3 system is higher than that of the NaSCN/NH_3 system.

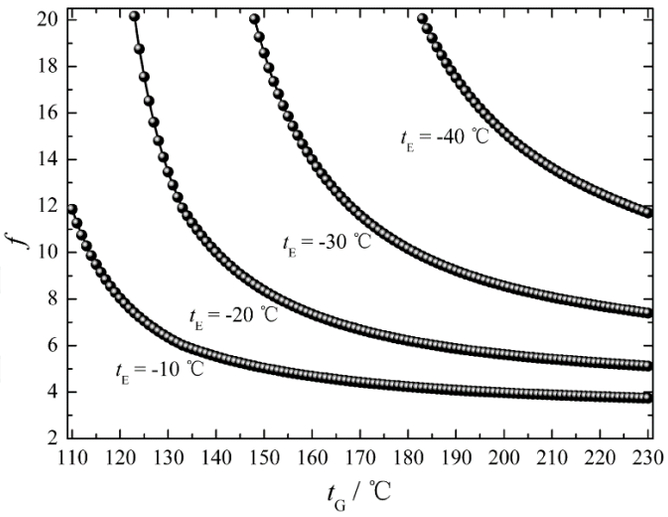


Figure 24. Effects of t_G on f for t_G = 110–230 °C, t_A = t_C = 35 °C and t_E= -10 °C, -20 °C, -30 °C, or -40 °C [25].

Fig. 24 shows effects of t_G on the f for t_G = 110–230 °C with t_A = t_C = 35 °C and t_E= -10 °C, -20 °C, -30 °C, or -40 °C. With an increase in t_G, the f declines, because the increase in t_G is conducive to desorption of NH_3 in the generator. With an increase in t_E, the f grows, because the increase in t_E will decrease the absorption pressure of the absorber. Thus, the absorption ability of the absorber will be decreased. The f is an important parameter for absorption refrigeration. An increase in the f will lead to an increase in the amount of energy used to heat the solution from t_A to t_G. If the f is greater than 10, the COP decreases, even when the efficiency of the regenerator is greater than 0.9. For t_E = -10 °C, -20 °C, and -30 °C, the circulation ratios are less than 10 when t_G is greater than 115°C, 139 °C, or 187 °C, respectively. Based on the results shown in Figs. 23 and 24, the [bmim]Zn_2Cl_5/NH_3 system can be used when t_E = -10 to -30 °C.

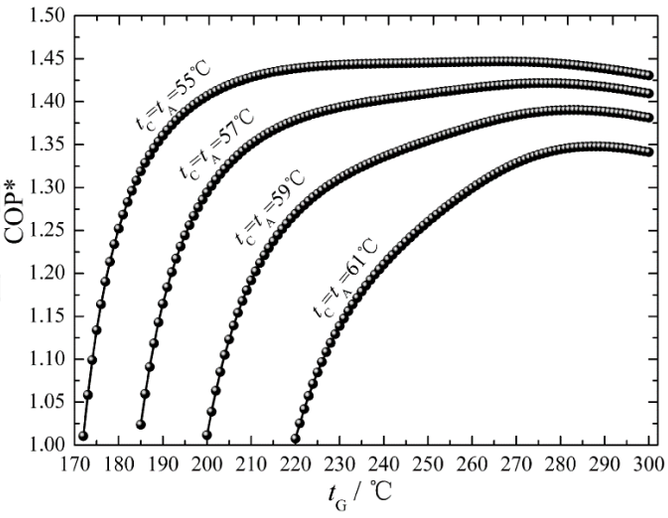


Figure 25. Effects of t_G on the COP* for t_G = 170–300 °C with t_A = t_C = 55 °C, 57 °C, 59 °C, or 61 °C and t_E = -10 °C [25].

Fig. 25 shows the effects of t_G on the COP* for t_G = 170–300 °C with t_A = t_C = 55 °C, 57 °C, 59 °C, or 61 °C and t_E = -10 °C. The COP* presents a trend of declining after increasing with an increase

in t_G. For $t_A = t_C$ = 55 °C, 57 °C, 59 °C, and 61 °C, the maximum COP* values of 1.447, 1.422, 1.390, and 1.348 appear at t_G =266 °C, 276 °C, 283 °C, and 289 °C, respectively. The COP* decreases with increases in t_A and t_C, because the increase in t_A is not conducive to absorption of NH_3 in the absorber. In addition, the increase in t_C is not conducive to desorption of NH_3 in the generator.

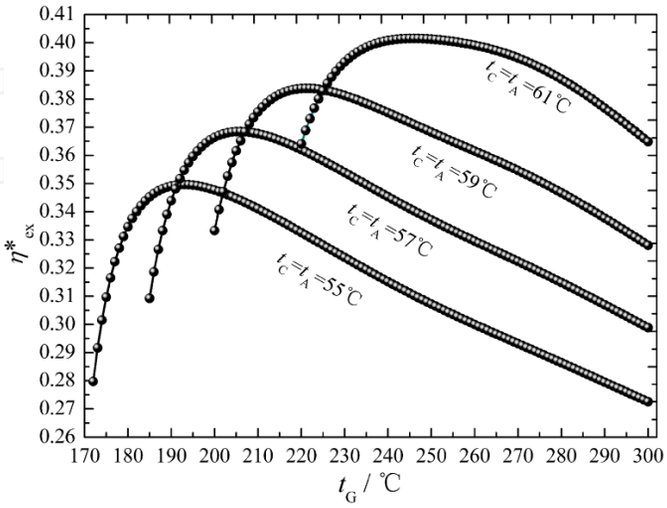


Figure 26. Effects of t_G on η^*_{ex} for t_G = 170–300 °C with $t_A = t_C$ = 55 °C, 57 °C, 59 °C, or 61 °C and t_E= -10 °C [25].

Fig. 26 shows the effects of t_G on η^*_{ex} for t_G = 170–300 °C with $t_A = t_C$ = 55 °C, 57 °C, 59 °C, or 61 °C and t_E= -10 °C. With an increase in t_G, the η^*_{ex} presents a trend of decreasing after initially increasing. For $t_A = t_C$ = 55 °C, 57 °C, 59 °C, and 61 °C, the maximum values of η^*_{ex} of 0.341, 0.368, 0.384, and 0.402 appear at t_G =193 °C, 206 °C, 221 °C, and 246 °C, respectively. It can be seen that the optimalη^*_{ex} occurs at a lower t_G than did the optimal COP*. This is because the increase in t_G leads to an increase in the exergy proportion in q_E, which induces a decreasing trend in η^*_{ex} but has no effect on the COP*.

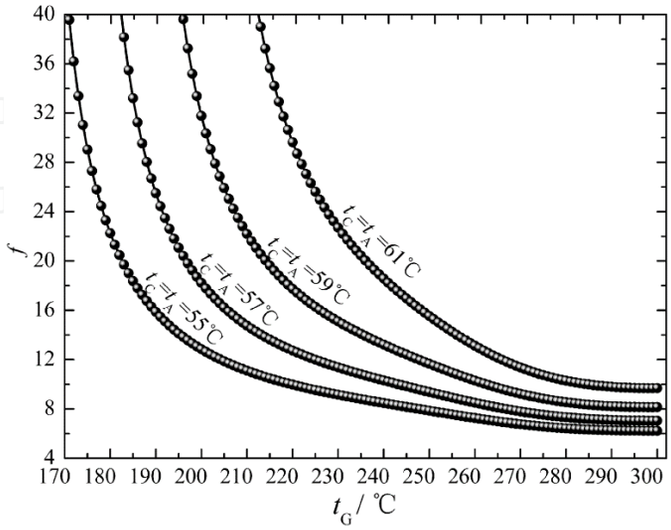


Figure 27. Effects of t_G on the f for t_G = 170–300 °C with $t_A = t_C$ = 55 °C, 57 °C, 59 °C, or 61 °C and t_E= -10 °C [25].

Fig. 27 shows the effects of t_G on the f for t_G = 170–300 °C with $t_A = t_C$ = 55 °C, 57 °C, 59 °C, or 61 °C and t_E= -10 °C. The variation in the f is the same as that for the COP for cooling in Fig. 6. For $t_A = t_C$ = 55 °C, 57 °C, 59 °C, and 61 °C, the f values are less than 10 when t_G is greater than 220 °C, 244 °C, 263 °C, and 285 °C, respectively. Overall, the results in Figs. 21–27 indicate that the [bmim]Zn_2Cl_5/NH_3 absorption system is suitable for use in heating applications.

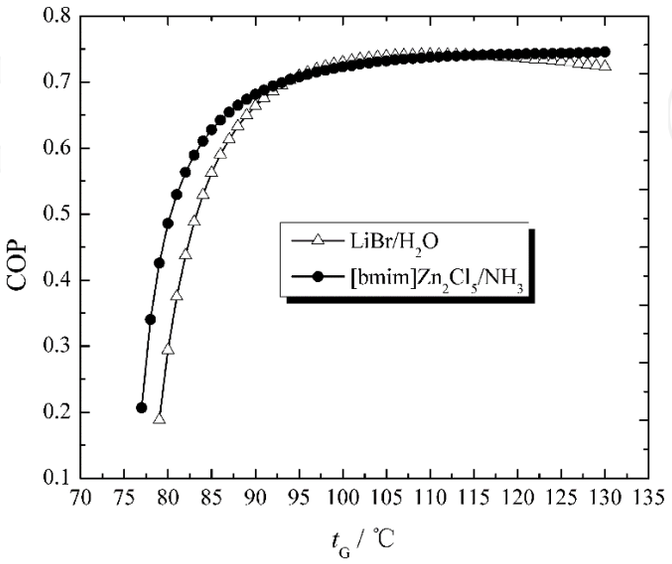


Figure 28. Effects of t_G on the COP for t_G = 75–130 °C with t_A = 35°C, t_C = 40 °C, and t_E = 5 °C.

The theoretical cycle characteristic of the [bmim]Zn_2Cl_5/NH_3 absorption system is also compared with that of the LiBr/H_2O system. Fig. 28 shows the effects of t_G on the COP for t_G = 75–130 °C with t_A = 35°C, t_C = 40 °C, and t_E = 5 °C and a heat recovery rate of the regenerator of 0.75. For both systems, the COP initially exhibits a significant increase as the t_G increases. As t_G continues to increase though, the slope of the COP curve for the [bmim]Zn_2Cl_5/NH_3 system becomes less steep, whereas the COP curve for the LiBr/H_2O system presents a trend of a slight decrease after the increase. When t_G < 95°C, the COP of the [bmim]Zn_2Cl_5/NH_3 system is slightly higher than that of the LiBr/H_2O system. When 95 < t_G < 115 °C, the COP of the [bmim]Zn_2Cl_5/NH_3 system is slightly less than that of the LiBr/H_2O system. When t_G > 115 °C, the COP of the [bmim]Zn_2Cl_5/NH_3 system is higher than that of the LiBr/H_2O system. As t_G continues to increase, the COP curve for the [bmim]Zn_2Cl_5/NH_3 system still maintains the upward trend with a small slope, but the COP curve of the LiBr/H_2O system shows a downward trend with a small slope. Although the COP of the [bmim]Zn_2Cl_5/NH_3 system is less than the COP of the LiBr/H_2O system at some specific temperatures, the overall theoretical cycle characteristic of the [bmim]Zn_2Cl_5/NH_3 system is slightly better than that of the LiBr/H_2O system, especially at higher t_G values.

3.5. Summary

The vapor pressures of the binary solution of [bmim]Zn_2Cl_5/NH_3 with NH_3 mole fraction x_2 = 0.83–0.94 at T = 323.15–563.15 K were measured via a static method with a total uncertainty of measurement below 4.3% [16]. The experimental data were fit using the modified UNIFAC

model, and new group interaction parameters between any two of the four tested groups were obtained with a maximum deviation less than 5% [16]. Vapor pressures were compared between $ZnCl_2$ $6NH_3$, ammonia solutions containing normal ionic liquids ([emim][Ac], [emim][SCN], [emim][$EtOSO_3$] and [DMEA][Ac]), and [bmim]Zn_2Cl_5/NH_3. The results indicate that the absorption characteristics of [bmim]Zn_2Cl_5 are much better than those of normal ionic liquids but slightly lower than those of $ZnCl_2$. However, the liquid form of [bmim]Zn_2Cl_5 offers a major advantage over $ZnCl_2$. Therefore, working pairs of [bmim]Zn_2Cl_5/NH_3 have good latent application in absorption refrigerator and heat pump operation.

TG scanning of [bmim]Zn_2Cl_5 was carried out using a TGA/SDT instrument over the range of T = 323.15–1173.15 K. The results indicate that [bmim]Zn_2Cl_5 possesses high thermal stability for T < 637.15 K. Heat capacity data at T = 210.15–383.15 K were obtained by using a DSC 910S operated with a rate of temperature increase of 5 $Kmin^{-1}$ and a nitrogen volume flow of 40 cm^3min^{-1}. Molar excess enthalpy data for [bmim]Zn_2Cl_5/NH_3 at x_1 = 0.60–0.95 for T = 288.15, 303.15, 318.15, and 333.15 K were measured. The excess enthalpy data were fit using the NRTL model. Measurement uncertainties and the maximum deviation of correlations for the excess enthalpy data were lower than 4.8% and 3.9%, respectively. With an increase in the NH_3 mole fraction, excess enthalpy showed a trend of increasing after declining. Minimum excess enthalpies of -6555.7, -6707.1, -6846.3, and -6974.7 J/mol appeared at x_1 = 0.772, 0.774, 0.776, and 0.777 for T = 288.15, 303.15, 318.15, and 333.15 K, respectively. Based on the heat capacity of [bmim]Zn_2Cl_5 and the excess enthalpy of [bmim]Zn_2Cl_5/NH_3, the enthalpies of [bmim]Zn_2Cl_5/NH_3 solutions can be calculated, which makes it feasible to investigate the thermodynamic performances of the [bmim]Zn_2Cl_5/NH_3 absorption system.

Based on the modified UNIFAC model and the NRTL model, the thermodynamic performance of a single effect absorption system using [bmim]Zn_2Cl_5/NH_3 as the working pair was simulated and compared with those of the $NaSCN/NH_3$ adsorption system [25] and the H_2O-LiBr absorption system. The thermal performance of the [bmim]Zn_2Cl_5/NH_3 system is better than that of the $NaSCN/NH_3$ system when the t_G is high and t_A and t_C are low and also better than that of the H_2O-LiBr absorption system in some cases. With an increase in t_G, the COP and COP* present trends of declining after increasing, and the circulation ratios show a decreasing trend. When t_E = -30 °C and t_A = t_C =35 °C, the maximum COP of the [bmim]Zn_2Cl_5/NH_3 system is still greater than 0.42. When t_E = -10 °C and t_A = t_C = 60 °C, the maximum COP* is still greater than 1.40. Under these two operating conditions, the circulation ratios remain acceptable. Although the COP of the [bmim]Zn_2Cl_5/NH_3 system is less than that of the $LiBr/H_2O$ system in some specific temperature ranges, the overall theorertical cycle characteristic of the [bmim]Zn_2Cl_5/NH_3 system is slightly better than that of the $LiBr/H_2O$ system, especially when t_G is high. Overall, these results indicate that the [bmim]Zn_2Cl_5/NH_3 absorption system offers good thermal performance for use in both cooling and heating applications.

4. Conclusions and outlook

Ten years have passed since ionic liquids were introduced in the field of absorption refrigeration, and unfortunately, the research progress pertaining to absorption refrigeration working pairs containing ionic liquids has been disappointing to us. Most of the working pairs proposed

by researchers from all over the world are gradually fading from view due to a lack of practical applications. Particular attention was paid to ionic liquid working pairs containing [RR'Im]DMP (1-R,3-R'-imidazolium dimethylphosphate). When applied in absorption refrigeration, the cycle characteristics of the three representative working pairs of [dmIm]DMP-H_2O, [emIm]DMP-H_2O and [mmIm]DMP-CH_3OH are better than that of H_2O-NH_3, but still slightly lower than those of LiBr-H_2O. So far, the new conceptual chemical absorption refrigeration working pairs containing an ionic liquid, with [bmim]Zn_2Cl_5/NH_3 as the representative, are the most ideal ionic liquid-type working pairs for absorption refrigeration. The thermodynamic performances of absorption refrigeration using the proposed chemical working pairs are comparable to those achieved with the LiBr-H_2O system. Additionally, the ranges of operating conditions for the chemical working pairs are wider than those of the conventional working pairs. At present, promoting the industrial application of [bmim]Zn_2Cl_5/NH_3 is our next priority. The discovery of chemical absorption refrigeration working pairs containing an ionic liquid is a milestone in the development of absorption refrigeration technology. It is foreseeable that the application of ionic liquids in absorption refrigeration will achieve a major breakthrough in the development of this technology, with the continued discovery of similar ionic liquid working pairs based on the chemical reaction.

Acknowledgements

This work was supported by the National Basic Research Program of China (973 Program) under Grant No. 2015CB251503 and the National Natural Science Foundation of China under Grant No. 51276180.

Author details

Shiqiang Liang[1*], Wei Chen[2], Yongxian Guo[1] and Dawei Tang[1]

*Address all correspondence to: liangsq@mail.etp.ac.cn

1 Institute of Engineering Thermophysics, Chinese Academy of Sciences, Beijing, P.R. China

2 College of Electromechanical Engineering, Qingdao University of Science and Technology, Qingdao, P.R. China

References

[1] S Q Liang, W Chen, K Y Cheng et al. The latent application of ionic liquids in absorption refrigeration. In: Application of ionic liquid in science and technology. InTechOpen, Croatia 2011:467-494.

[2] J Zhao, S Q Liang, J Chen, et al. VLE for the High Concentration [MMIm]DMP-Methanol Solutions. Chemical Engineering, 38 (2010) 52-56

[3] J Zhao, X C Jiang, C X Li. Vapor Pressure Measurement for Binary and Ternary Systems Containing a Phosphoric Ionic Liquid. Fluid Phase Equilibria, 247 (2006) 190-198.

[4] W Chen, S Q Liang, Y X Guo et al. Thermodynamic performances of [mmim]DMP/methanol absorption refrigeration. Journal of Thermal Science, 21 (2012) 557-563.

[5] L Dong, D X Zheng, N Nie et al. Performance prediction of absorption refrigeration cycle based on themeasurements of vapor pressure and heat capacity of H_2O + [DMIM]DMP system. Applied Energy, 98 (2012) 326-332.

[6] J Ren, Z C Zhao, X D Zhang. Vapor pressures, excess enthalpies, and specific heat capacities of the binary working pairs containing the ionic liquid 1-ethyl-3-methylimidazolium dimethylphosphate, Journal of Chemical Thermodynamics, 43(2011) 576-583.

[7] X D Zhang, D P Hu. Performance simulation of the absorption chiller using water and ionic liquid 1-ethyl-3-methylimidazolium dimethylphosphate as the working pair. Applied Thermal Engineering, 31 (2010) 3316-3321.

[8] R Z Wang, L W Wang. Adsorption refrigeration- green cooling driven by low grade thermal energy. Chinese Science Bulletin, 50 (2005) 193-204.

[9] K Wang. Performance and application of $CaCl_2$/expanded graphite adsorbent for double heat pipes type refrigeration. Ph. D dissertation of Shanghai Jiao Tong University, Shanghai, 2007.

[10] L W Wang, R Z Wang, J Y Wu. Design of heat pipe type adsorption ice-making for fishing boats. Journal of Chemical Engineering, 13 (2005) 403-410.

[11] T X Li, R Z Wang, R G Oliveira. Performance analysis of an innovative multimode, multisalt and multieffect chemisorption refrigeration system. Journal of American Institute of Chemical Engineers, (2007) 3222-3230.

[12] Y Wei, Q G Zhang. Properties of ionic liquid based on zinc chloride $BMIZn_2Cl_5$. Acta Chemica Sinica, 66 (2008) 1879-1883.

[13] M B Meredith, C H McMillen, J T. Goodman. Ambient temperature imidazolium-based ionic liquids with tetrachloronickelate(II) anions. Polyhedron, 28(2009) 2355-2358.

[14] I Lin, C S Vasam. Metal-containing ionic liquids and ionic liquid crystals based on imidazolium moiety. Journal of Organometallic Chemistry 690 (2005) 3498-3512.

[15] W Guan, L Li, H Wang et al. Studies on thermochemical properties of ionic liquids based on transition metal. Journal of Thermal Analysis and Calorimetry, 94 (2008)507-510.

[16] W Chen, S Q Liang, Y X Guo et al. Investigation on vapor-iquid equilibria for binary systems of metal ion-containing ionic liquid [bmim]Zn_2Cl_5/NH_3 by experiment and modified UNIFAC model. Fluid Phase Equilibria, 360 (2013) 1-6.

[17] A W Islam, M H Rahman. A review of Barker's activity coefficient method and VLE data reduction. Journal of Chemical Thermodynamics, 44 (2012) 31-37.

[18] S Li, Z L Cheng, Y Q Ma et al. The new concise equation of state for ammonia. Journal of Engineering Thermophysics, 21 (2000) 17-19.

[19] A Yokozeki, M B Shiflett. Vapor-liquid equilibria of ammonia + ionic liquid mixtures. Applied Energy, 84 (2007) 1258-1273.

[20] R S Santiagoa, G R Santos, M Aznar. Liquid-liquid equilibrium in ternary ionic liquid systems by UNIFAC: new volume, surface area and interaction parameters. Fluid Phase Equilibria, 295 (2010) 93-97.

[21] L Lemos, P Patrício, G Rodrigues et al. Liquid-liquid equilibrium of aqueous two-phase systems composed of poly(ethylene oxide) 1500 and different electrolytes ($(NH_4)_2SO_4$, $ZnSO_4$ and K_2HPO_4): Experimental and correlation. Fluid Phase Equilibria, 305 (2011) 19-24.

[22] J A Gonzalez, I G Fuenta, J C Cobos. Thermodynamics of mixtures with strongly negative deviations from Raoult's Law Part 4. Application of the DISQUAC model to mixtures of 1-alkanols with primary or secondary linear amines. Comparison with Dortmund UNIFAC and ERAS results. Fluid Phase Equilibria, 168 (2000) 31-58.

[23] L Chen, S H Yu, Y K Tan. An experimental study on the adsorption refrigeration characteristics of ammonia. Journal of Refrigeration, 4 (2000) 18-22.

[24] H Renon, J M Prausnitz. Local compositions in thermodynamic excess functions for liquid mixtures. Journal of American Institute of Chemical Engineers, 14 (1968) 135-144.

[25] W Chen, S Liang, Y Guo, D Tang. Thermodynamic analysis of an absorption system using [bmim]Zn_2Cl_5/NH_3 as the working pair. Energy Conversion and Management, 85 (2014) 13-19.

[26] L H Zhu, J J Gu. Second law-based thermodynamic analysis of ammonia/sodium thiocyanate absorption system. Renewable Energy, 35 (2010) 1940-1946.

[27] L G Farshi, C A I Ferreira, S M S Mahmoudi et al. First and second law analysis of ammonia/salt absorption refrigeration systems. Journal of Refrigeration, 40 (2014) 111-121.